European Journal of Pharmaceutics and Biopharmaceutics 141 (2019) 161–171

Contents lists available at ScienceDirect

European Journal of Pharmaceutics and Biopharmaceutics

journal homepage: www.elsevier.com/locate/ejpb

Research paper

# The obstacle course to the inner retina: Hyaluronic acid-coated lipoplexes cross the vitreous but fail to overcome the inner limiting membrane

Joke Devoldere[a], Mike Wels[a], Karen Peynshaert[a], Heleen Dewitte[a,b,c], Stefaan C. De Smedt[a,c], Katrien Remaut[a,c,*]

[a] Ghent Research Group on Nanomedicines, Laboratory of General Biochemistry and Physical Pharmacy, Ghent University, Ottergemsesteenweg 460, 9000 Ghent, Belgium
[b] Laboratory for Molecular and Cellular Therapy, Department of Biomedical Sciences, Medical School of the Vrije Universiteit Brussel (VUB), Laarbeeklaan 103, 1050 Jette, Belgium
[c] Cancer Research Institute Ghent (CRIG), Ghent University Hospital, De Pintelaan 185, 9000 Ghent, Belgium

ARTICLE INFO

*Keywords:*
Hyaluronic acid
Coating
Müller cells
Lipoplexes
mRNA
Ocular
Intravitreal
Drug delivery
Retina
Inner limiting membrane

ABSTRACT

Considerable research over the last few years has revealed dysregulation of growth factors in various retinal diseases, such as glaucoma, diabetic retinopathy and photoreceptor degenerations. The use of messengerRNA (mRNA) to transiently overexpress a specific factor could compensate for this imbalance. However, a critical challenge of this approach lies in the ability to efficiently deliver mRNA molecules to the retinal target cells. In this study we found that intravitreal (IVT) injection is an attractive approach to deliver mRNA to the retina, providing two critical barriers can be overcome: the vitreous and the inner limiting membrane (ILM). We demonstrated that the vitreous is indeed a major hurdle in the delivery of the cationic mRNA-complexes to retinal cells, both in terms of vitreal mobility and cellular uptake. To improve their intravitreal mobility and avoid unwanted extracellular interactions, we evaluated the use of hyaluronic acid (HA) as an electrostatic coating strategy. This HA-coating provided the complexes with a negative surface charge, markedly enhancing their mobility in the vitreous humor, without reducing their cellular internalization and transfection efficiency. However, although this coating strategy allows the mRNA-complexes to successfully overcome the vitreal barrier, the majority of the particles accumulated at the ILM. This study therefore underscores the crucial barrier function of the ILM toward non-viral retinal gene delivery and the need to smartly design mRNA-carriers able to surmount the vitreous as well as the ILM.

## 1. Introduction

The development of mRNA-based medicine was long deemed inferior to the creation of gene therapeutics based on DNA. Nowadays, *in vitro*-transcribed mRNA is reviving as a promising candidate for the delivery of genetic information. Recent investments in improving mRNA synthesis and stability have enabled a wide range of applications, thereby even surpassing the potential that was once envisioned for DNA-based medicine [1]. With regard to ocular delivery, mRNA offers several key advantages in comparison to DNA-based gene therapeutics. Since it can be instantly translated in the cytoplasm without the need for nuclear entry [2], mRNA is an ideal candidate for the transfection of post-mitotic retinal cells. In view of safety concerns, mRNA does not integrate into the host genome, which reduces the risk of insertional mutagenesis. In addition, complete physiological degradation provides mRNA with a transient activity, providing a more controlled temporal expression [3]. Together, these advantages could allow mRNA to safely induce the local expression of various substances in the retina, such as anti-apoptotic proteins [4,5], ROS inhibitors or neurotrophic factors [6-10] that could slow down retinal degeneration of many ocular diseases.

The success of *in vivo* IVT-mRNA will greatly depend on its ability to overcome the extracellular barriers that precede mRNA delivery to the retinal target cells. In this regard, intravitreal (IVT) administration provides an attractive administration route, bypassing the blood ocular barriers and delivering the mRNA in close proximity to the target site.

*Abbreviations:* AMD, age-related macular degeneration; DLS, dynamic light scattering; FCS, fluorescence correlation spectroscopy; fSPT, fluorescence single particle tracking; GAG, glycosaminoglycan; HA, hyaluronic acid; ILM, inner limiting membrane; IVT, intravitreal; MW, molecular weight; NA, nucleic acid; PDI, polydispersity index; PEG, polyethylene glycol; SLN, solid lipid nanoparticle; SV, sonicated vitreous; VR, vitreoretinal

* Corresponding author at: Ghent Research Group on Nanomedicines, Ghent University, Ottergemsesteenweg 460, B9000 Ghent, Belgium.
*E-mail address:* Katrien.Remaut@ugent.be (K. Remaut).

https://doi.org/10.1016/j.ejpb.2019.05.023
Received 20 February 2019; Received in revised form 27 May 2019; Accepted 27 May 2019
Available online 28 May 2019
0939-6411/ 

In the clinic, IVT injections are routinely performed for the administration of a wide range of drugs, in particular monoclonal antibodies, which are injected on a daily base for the treatment of age-related macular degeneration (AMD). Also for gene delivery, IVT injections are a widely investigated injection route, especially when (widespread) delivery to the inner retina is desired (to reach targets such as Müller cells or retinal ganglion cells (RGCs)) [6,11]. Even though IVT administration delivers drugs directly into the vitreous chamber of the eye, several extracellular barriers still need to be considered before effectively reaching the target site. Indeed, a first barrier hampering IVT-mediated gene delivery is the vitreous itself. Following IVT injection, naked nucleic acids will be exposed to nucleases present in the vitreous humor [12]. In order to circumvent this issue, research has been conducted to package nucleic acids (NAs) into vectors that protect them from IVT degradation and that facilitate uptake in the retinal cells [13,14]. However, when designing suitable carriers, it should be taken into account that the vitreal network can interfere with the diffusion of these carriers and prevent their migration to the retina [11,15–17]. A second barrier to keep in mind, is the inner limiting membrane (ILM), which represents the structural boundary between the vitreous and the retina. Although most studies with non-viral vectors document efficient penetration of particles in the retina of rodents [18,19], retinal delivery via IVT injection is rarely successful in larger animals; likely because most carriers fail to overcome the more complex barriers present in larger species [20].

In this work we therefore make use of two *ex vivo* bovine models, more representative for human physiology, to investigate the most important extracellular barriers that impede delivery of mRNA to the retina after IVT injection. The first model comprises a bovine eye, removed of its anterior parts, which is designed to visualize the diffusion of vectors in the intact vitreous body by means of high-resolution microscopy [21]. The second model consists of the retina to which, in contrast to other existing explant models, the vitreous is maintained at all times in order to study the role of the preserved vitreoretinal interface as a barrier for retinal vector delivery [22]. In these models, we evaluate the use of the cationic non-liposomal polymer/lipid formulation *Trans*IT™ for the delivery of mRNA towards the retina. TransIT™ is composed of two components, the TransIT®-mRNA Reagent and mRNA Boost Reagent, both specifically designed for efficient mRNA complexation. To shield the surface of positively charged particles from interaction with the vitreal constitutes, surface coating with polyethylene glycol (PEG) has been previously suggested [21]. However, PEG is known to pose steric hindrance, thereby impeding interactions of the complexes with cell membranes and subsequently reducing uptake by the target cells [26,27]. In the present study, an alternative coating strategy by means of hyaluronic acid (HA) is tested. HA is an anionic, biodegradable biopolymer, which is abundantly present in the vitreous humor and widely distributed throughout the retina [28,29]. We study the effect of HA-coating on the capacity of the *Trans*IT-complexes to encapsulate mRNA and on the mobility and the transfection efficiency of these particles in the bovine vitreous. As retinal target, Müller cells are chosen since their endfeet are in close contact to the vitreous, making them one of the first cell types to be encountered following IVT injection [38]. Finally, we look into the competence of these particles to carry the mRNA across the vitreoretinal (VR) interface and highlight the individual barrier role of both vitreous and ILM for retinal non-viral mRNA delivery.

## 2. Materials and methods

### 2.1. mRNA

Unmodified enhanced green fluorescent protein (eGFP)-encoding mRNA was produced by *in vitro* mRNA transcription from pGEM4Z-GFP-A64 plasmids. eGFP was chosen as reporter protein to allow quantitative determination of gene expression by flow cytometry (yielding bright green fluorescence with an emission peak at 509 nm). The plasmids were purified using a QIAquick PCR purification kit (Qiagen, Venlo, The Netherlands) and linearized using the Spe I restriction enzyme (Promega, Leiden, The Netherlands). Linearized plasmids were used as templates for the *in vitro* transcription reaction using the mMESSAGE mMACHINE T7 transfection kit (Ambion, Life Technologies, Ghent, Belgium), including a 7-methylGpppG cap analog. Subsequently, mRNAs were treated with DNase I and purified using the RNeasy Mini Kit (Qiagen). The mRNA concentration was determined by measuring the absorbance at 260 nm. mRNA was stored in small aliquots at −80 °C at a concentration of 1 μg μl$^{-1}$. To label the mRNA for FCS measurements, a 10 μM solution of YOYO-1 iodide (Molecular Probes, Merelbeke, Belgium) was added to the eGFP encoding mRNA in a 10:1 bp to dye ratio, corresponding with a mixing ratio of 15:1 dye to mRNA (v/w). The mixture was incubated for 4 h at room temperature (RT) and the labeled mRNA was purified by addition of 2.5 volumes ice-cold ethanol and 0.1 vol of 5 M NaCl. Following incubation at −80 °C the sample was centrifuged (30 min at 17,000*g*) and washed with 70% ethanol. Finally the pellet was resuspended in RNase free water and the concentration of the fluorescently labeled mRNA was again measured by UV absorption at 260 nm. For microscopy experiments, the mRNA was fluorescently labeled with Cy®5 using the Label IT® Nucleic Acid Labeling kit of Mirus Bio (Madison, WI). Cy5 was added to the mRNA in a ratio of 1:1 (v:w). The mixture was incubated for 1 h at RT and the labeled mRNA was purified according to the manufacturer's instructions by means of G50 microspin purification columns.

### 2.2. mRNA complexation

mRNA was complexed to the *Trans*IT transfection reagent (Mirus Bio, Madison, WI) according to the manufacturer. To determine the mRNA complexation efficiency of *Trans*IT by gel electrophoresis, mRNA was mixed with the *Trans*IT-mRNA reagent and mRNA boost reagent in different volume (μl) to weight (μg) ratios. All complexes were prepared in a final volume of 10 μl Opti-MEM™ (Thermo Scientific). An optimal ratio of mRNA (0.09 μg), *Trans*IT-mRNA reagent (0.18 μl), and Boost reagent (0.18 μl) was chosen for all further experiments. When complexing different amounts of mRNA (μg) the finale volume and the volume of the reagents were scaled proportionally. For electrostatic HA-coating of the prepared complexes, the required amount of HA to achieve a certain HA/*Trans*IT/mRNA ratio (v/v/w) was diluted in RNase free water and added to an equal volume of *Trans*IT-mRNA complexes. In this ratio HA refers to the number of negative charges originating from the carboxyl groups of the HA-monomers. Following 10 s of vortexing, the suspension was incubated during 10 min at RT to stabilize. HA was purchased with three different molecular weights (MWs) of 20 kDa, 200 kDa and > 1.8 MDa according to the manufacturer. These samples were analyzed with gel permeation chromatography and are referred to as HA22, HA137 and HA2700 respectively, based on their weight-averaged MW distributions as reported earlier [37].

### 2.3. Gel electrophoresis

Coated and uncoated *Trans*IT-mRNA complexes were prepared as described above. For each desired v/w ratio (i.e. *Trans*IT/Boost reagent (μl) to mRNA (μg) ratio) an appropriate amount corresponding to 0.5 μg mRNA was incubated in Opti-MEM™, fetal bovine serum (FBS) or adult bovine vitreous (ABV). After 30 min incubation at 37 °C, 5 μl Ambion loading buffer was added and mixtures were loaded into a 1.2% agarose gel in TRIS/Borate/EDTA (TBE) buffer, to which GelRed (Biotium, Hayward, CA) was added for visualization of the mRNA. The gel was run for 40 min at 100 V and imaged by UV illumination and gel photography. A 0.5 to 10 kb RNA ladder (Thermo Scientific) was included. Samples containing free mRNA in Opti-MEM™, FBS or ABV were run as controls. To determine the complexation efficiency gel analysis was

performed using the ImageJ software (NIH).

### 2.4. Physical characterization of the complexes

Size distribution and zeta potential of the *Trans*IT-mRNA complexes were measured by dynamic light scattering (DLS) using a Malvern Zetasizer nano-ZS (Malvern Instruments, Worcestershire, UK). All samples were diluted in 20 mM HEPES buffer pH 7.4 (Sigma-Aldrich). Size measurements were done in triplicate, with three runs per replicate and presented as number averaged hydrodynamic diameter. Zeta potential measurements were done in triplicate with two runs per replicate.

### 2.5. Fluorescence single particle tracking (fSPT) microscopy

To determine the diffusion of the complexes in an aqueous environment, *Trans*IT-complexed Cy5-labeled mRNA was diluted in RNase free HEPES buffer (20 mM, pH 7.4, Sigma-Aldrich) to a concentration of $10^8$ to $10^9$ complexes per ml. Fifty μl of the samples was transferred into a 96-well microplate (Greiner Bio-One, Vilvoorde, Belgium) and the mobility of the complexes was measured with fluorescence single particle tracking (fSPT) microscopy. fSPT is based on microscopic imaging of fluorescently labeled single molecules to characterize their diffusion. Real-time confocal tracking of individually moving lipoplexes allows to calculate their motion trajectories and diffusion coefficient. All fluorescence video imaging of diffusing lipoplexes was performed on a swept-field confocal microscope (LiveScan Swept Field Confocal Microscope System; Nikon, Brussels, Belgium) equipped with a Plan Apo 100× 1.4 NA oil immersion objective lens (Nikon) and a fast and sensitive EMCCD camera (Ixon Ultra 897, Andor Technology, CT, USA). The microscope was focused at 5–10 μm above the bottom of the well plate and the Cy5-labelled mRNA lipoplexes were excited with a solid-state 125 mW 640 nm (Agilent Technologies, CA, USA) laser. For each sample, typically 25 movies of about 100 frames each were recorded at different random locations within the sample.

To measure the diffusion of uncoated and HA-coated *Trans*IT-mRNA complexes in intact vitreous, SPT was performed in an *ex vivo* model as previously described by Martens et al. [21]. In summary, fresh bovine eyes were obtained from a local abattoir, disposed of extra-ocular material, disinfected in 20% ethanol and washed in sterile $CO_2$ independent medium. Subsequently, cornea and lens were removed, exposing the hyaloid membrane that holds the vitreous. A volume of 30 μl with a concentration of 50 ng $\mu l^{-1}$ Cy-5 labelled mRNA was injected at four different places in the vitreous as close as possible to the hyaloid membrane. Next, the complete eye was transferred to a glass bottom dish (In Vitro Scientific, Mountain View, CA) with the hyaloid membrane positioned against the glass bottom allowing visualization of the vitreous by fluorescence microscopy. Finally, the samples were stored at RT for 24 h permitting the diffusion of particles through the vitreous. Particle mobility was determined by fSPT. Diffusion analysis of all videos was performed using in-house developed software, as described before [39], providing a distribution of apparent diffusion coefficients.

### 2.6. Cell culture and transfections

The human Müller cell line Moorfields/Institute of Ophtalmology-Müller 1 (MIO-M1) was obtained from the UCL Institute of Ophthalmology, London, UK [40]. The cells were cultivated in Dulbecco's Modified Eagle's Medium (DMEM) GlutaMax®pyruvate 1 g $l^{-1}$ glucose (Gibco-Invitrogen) supplemented with 1% L-glutamin, 2% penicillin/streptomycin and 10% FBS (Hyclone). Cells were passaged at 90% confluency and incubated at 37 °C with 5% $CO_2$. Five days prior to transfection, cells were seeded on 0.4 μm pore membrane inserts (Greiner Bio-One, Vilvoorde, Belgium) at $6.10^3$ cells/insert in a 12 well plate. Culture medium was added below the insert to assure optimal cell viability. Either culture medium or bovine vitreous was applied on top of the cells. For the latter fresh bovine eyes were obtained from a local abattoir, cleaned from extra-cellular tissue, washed with 20% ethanol and bisected. The vitreous was isolated and sonicated using a tip sonicator (Branson, Swedesboro, NJ) for 3 min with short intervals every 30 s to allow fluent pipetting. Naked or complexed mRNA was added to the culture medium or the vitreous at a concentration of 0.5 μg mRNA per $1x10^5$ cells. Afterwards cells were incubated at 37 °C during 3 or 24 h, for uptake or transfection experiments respectively.

### 2.7. Flow cytometry

Flow cytometric analysis was conducted on MIO-M1 that were transfected with naked or *Trans*IT-complexed eGFP mRNA (green; emission 509 nm) as described above. For uptake experiments eGFP mRNA was labeled with Cy®5 (far red; emission 670 nm). Cells treated with 50 μl Opti-MEM™ alone or cells treated with the same amount of *Trans*IT complexes containing fLuc-encoding mRNA were used as negative controls. The cells were detached from the plate surface with 0.25% trypsin-EDTA (Gibco, Paisly, UK), washed with cell culture medium and resuspended in PBS supplemented with 0.1% sodium azide and 1% bovine serum albumin. To allow identification of dead and apoptotic cells during the transfection experiments, respectively DAPI (blue; emission 461 nm) and MitoProbe™ $DiIC_1(5)$ (ThermoFischer) (far red; emission 658 nm) stainings were added to the cell suspension according to the manufacturer's instructions. After 30 min incubation at 37 °C, cells were analyzed using the CytoFLEX™ Flow Cytometer (Beckman Coulter, Krefeld, Germany) and data analysis was performed using FlowJo software (FlowJo, OR, USA). A minimum of 7000 gated cells was counted per tube. Percentages of eGFP-expressing cells were calculated from the percentage of the cell population that exceeded the fluorescence intensity of the control cells. Mean fluorescence intensity (MFI) was calculated for the entire viable cell population.

### 2.8. Fluorescence correlation spectroscopy (FCS)

To confirm the coating of complexes with HA, fluorescence correlation spectroscopy (FCS) was used. Green *Trans*IT-mRNA complexes were prepared using YOYO-labelled eGFP mRNA and coated with red labelled HA (Hyaluronate-DyLight® 650, 20 kDa, Creative PEGWorks, Chapel Hill, NC). The samples were measured with a confocal microscope equipped with a PicoHarp 300 FCS Unit (Picoquant, Berlin, Germany). A 60x water lens (Nikon, Brussel, Belgium) was used and the samples were measured for 60 s. A green and red laser transmitting at 488 nm and 640 nm respectively, with a laser intensity of 5% were used. The excited fluorescent particles were processed by a dual detector unit (Picoquant). The obtained photon count distributions were then analysed with the software symphotime (Picoquant).

### 2.9. Dissection and culture of a vitreoretinal bovine explant

Bovine retinal explants with an intact vitreoretinal interface, so-called "vitreoretinal (VR) explants", were prepared according to a protocol, recently developed in our lab [22]. This explant model differs from conventional explants by the preservation of vitreous and intact ILM during dissection. In short, an incubation period of 20–30 min in $CO_2$ independent medium at RT allowed gently warming of the bovine eye. Subsequently, the eye was bisected, the anterior segment was removed and a posterior eye cup filled with vitreous gel remained. Next, the retina was gently detached from the choroid at the rim of the eyecup and the vitreous was gently pulled down during which the attached retina came along. The whole tissue was transported with vitreous side upwards into a culture dish of 10 cm (Corning) filled with cold $CO_2$ independent medium and cut into three pieces of VR explant. A plastic Pasteur pipette was used to gently aspire one of the VR explant and transfer it to a dry 75 mm Transwell® explant filter (Corning). Excess amounts of vitreous was removed by aspiration and cutting and

20 ml of supplemented NeurobasalR-A medium is added below the explant filter. Twenty-five μg of Cy5-labeled eGFP mRNA complexed with *Trans*IT, was injected in the vitreous of the VR explants. Finally, explants were incubated for 24 h at 37 °C and 5% $CO_2$.

### 2.10. Cryosections

Bovine explants were fixed for 2 h at 4 °C in 4% paraformaldehyde and cryoprotected in 30% sucrose overnight at 4 °C. Next, tissues were embedded in OTC before snap freezing with liquid nitrogen. 10–12 μm sections of the frozen samples were cut at −21 °C using a cryostat (Leica Biosystems, Diegem, Belgium).

### 2.11. Immunostaining

Before staining, tissue sections were dried at RT, washed with PBS and permeabilized with a PBS-Triton 0.1% solution. Retinal sections were blocked in 1% normal goat serum and 0.05% Tween20 in PBS for 1 h at RT. For immunohistochemical staining of the ILM, sections were incubated at 4 °C overnight with a 1:200 dilution of rabbit antibody against Collagen IV (in blocking solution). After washing with PBS, the sections were incubated for 2 h at RT with goat anti-rabbit Alexa Fluor®488 (Abcam, 1:500 dilution). Slices were rinsed in PBS and counterstained with 1 μg $ml^{-1}$ Hoechst for 30 min at RT. Finally, samples were mounted with Vectashield (Vector Laboraties) and examined by confocal microscopy (C1-si, Nikon Belux, Brussels, Belgium) using a 60x oil objective (NIR Apo, Nikon).

### 2.12. Statistical analysis

All data are presented as mean ± standard deviation and are representative for at least 3 independent experiments conducted on 3 different days, unless stated otherwise. Experiments were analyzed for statistical significance with a one or two-way ANOVA followed by the Bonferroni post hoc test for significant differences between treated groups, or the Dunnett post hoc test when compared with a single control group. Statistical analysis was performed using Graphpad Prism 6 software (La Jolla, CA, USA). Asterisks indicate statistical significance ($^{*}p < 0.05$; $^{**}p < 0.01$; $^{***}p < 0.001$).

## 3. Results

### 3.1. Characterization of the TransIT-mRNA complexes

To guarantee complete protection of the mRNA against enzymatic degradation, we performed gel electrophoresis to examine mRNA complexation of *Trans*IT-mRNA complexes with a varying v/w ratio (i.e. *Trans*IT/Boost reagent (μl) to mRNA (μg) ratio) in biologically relevant media: Opti-MEM™, fetal bovine serum (FBS) and adult bovine vitreous (ABV) (Fig. 1A). From these gel electrophoresis experiments, we quantified the percentage of complexed mRNA using Image J software (Fig. 1B). As can be seen from Fig. 1A, free mRNA degrades in both FBS and bovine vitreous (lane 5 and 6). All *Trans*IT formulations keep the mRNA co-localized in the slots of the agarose gel, indicating that the mRNA does not dissociate after incubation in Opti-MEM™ (lane 7–10), serum (lane 11–14) or vitreous (lane 15–18) and hence full protection is offered against mRNA degradation. As suggested by the manufacturer a v/w ratio of 2 was selected for further experiments. At this v/w ratio the *Trans*IT-mRNA complexes exhibit a zeta potential of +25 mV (Fig. 3B) and display a bimodal size distribution (PDI = 0.374), with the highest frequency of complexes at 190 nm (Fig. 1C). The second peak at 712 nm indicates that a fraction (~43.7%) of the complexes tend to aggregate.

### 3.2. The vitreous as a barrier for intravitreal mRNA delivery

When evaluating complexes for IVT injection, it is essential to assure optimal mobility of the complexes throughout the vitreous and to minimize unspecific interactions with the vitreal components. In order to evaluate the mobility of the complexes in the vitreous humor, Cy5-labeled mRNA complexed with *Trans*IT was injected in an *ex vivo* model that contains intact bovine vitreous [21]. The movement of the complexes was visualized by single particle tracking (SPT) microscopy 24 h after injection and compared to their diffusion in HEPES buffer. From the distribution of the diffusion coefficients (Fig. 2A) we can derive that the complexes are substantially slowed down in vitreous (solid line) relative to their free diffusion in HEPES (dotted line). After IVT injection the complexes show a bimodal diffusion distribution with a high fraction of immobilized particles, which is in line with previously reported data for cationic lipid and polymer-based particles [19,21,24,25]. To evaluate whether the *Trans*IT-complexed mRNA retained its transfection potential in the presence of vitreous, we analyzed its uptake and transfection efficiency in MIO-M1 Müller cells in the presence of bovine vitreous versus culture medium. To this end MIO-M1 Müller cells were seeded on the permeable membrane of a Transwell® membrane to which mRNA-containing medium or sonicated vitreous (SV) was added. By allowing the cells to contact culture medium through the bottom of the transwell insert at all time, adequate nutrient supply and optimal cell viability can be ensured. It is important to note that in both uptake and transfection studies SV was used. While retaining all of its components, the collagen network in this vitreous is dismantled by sonication, resulting in a higher mobility of the particles compared to intact vitreous (Supplementary Fig. S1). As expected from the rapid mRNA degradation shown in Fig. 1A, Cy5-labeled naked mRNA failed to be taken up when added to either medium or vitreous (Fig. 2B). Subsequently no eGFP expression was induced in either culture condition (Fig. 2D). *Trans*IT-mRNA complexes, however, were taken up by nearly 50% of the cells when applied in culture medium (Fig. 2B). The presence of SV significantly decreased uptake of the complexes to 20% and resulted in a lower transgene expression compared to medium (Fig. 2D,E). Finally, cytotoxicity of the *Trans*IT-mRNA complexes was evaluated by quantifying the percentage of apoptotic and dead cells via $DiIC_1(5)$ and DAPI staining. From the data presented in Fig. 2C, we can conclude that *Trans*IT-mRNA complexes are well tolerated by the MIO-M1 Müller cells in both culture conditions. Taken together, even though the vitreal network is mechanically broken up, the vitreal content itself seems to form a significant barrier for *Trans*IT mediated mRNA delivery.

### 3.3. Optimization of HA-coating

Based on our observation that the mobility of cationic particles through the vitreous is hindered due to their interaction with the negatively charged components of the vitreous humor, we evaluated the use of HA to coat the complexes in order to shield their cationic surface. Additionally, since it is well-known that native HA has many different biological functions depending on its molecular weight (MW), we investigated the possible effect of MW on the electrostatically-coated HA-complexes by using HA with MWs of 22 kDa, 137 kDa and 2700 kDa. Size and zeta potential of the *Trans*IT-complexes were determined by dynamic light scattering (DLS) (Fig. 3A and B). Uncoated complexes were prepared by spontaneous complexation of the *Trans*IT reagent to the mRNA at a v/w ratio of 2:1, resulting in particles with a net positive surface charge. Electrostatic coating with increasing amounts of HA decreased the zeta potential, which inverted to a negative charge starting from a HA/*Trans*IT/mRNA ratio of 16:2:1 (v/v/w) (Fig. 3B). These results correlated well with the particle size: particles with a close to neutral surface charge tended to aggregate, resulting in a mean size of ~1000 nm, whereas a particle size of ~125 nm was maintained at a ratio of 16:2:1 (v/v/w) due to electrostatic repulsion between the

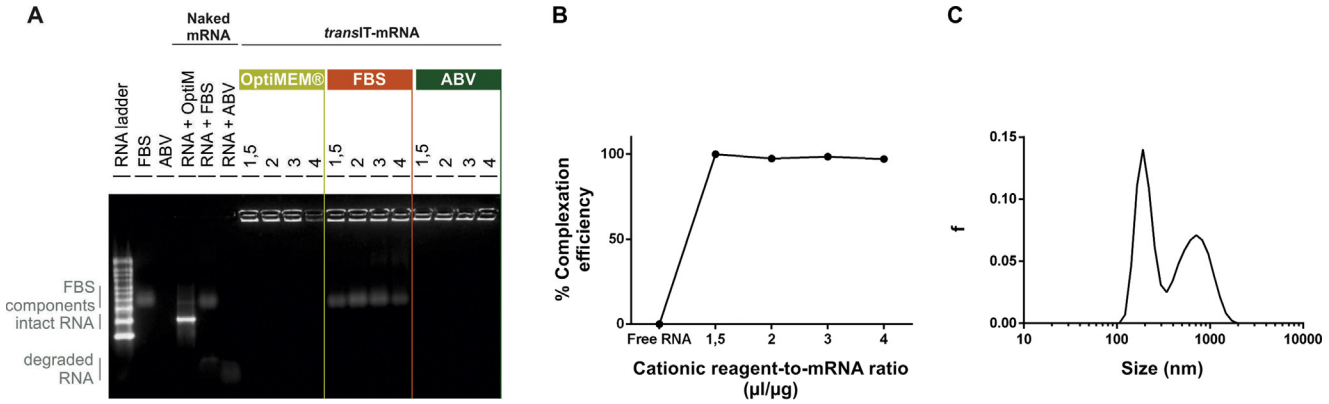


**Fig. 1. Characterization of the *Trans*IT-mRNA complexes.** (A) Gel electrophoresis on free mRNA and *Trans*IT-complexed mRNA demonstrates complete mRNA complexation at all studied v/w ratios in Opti-MEM™, fetal bovine serum (FBS) and adult bovine vitreous (ABV). A 0.5 to 10 kb molecular weight marker was included. (B) The percentage complexation efficiency in Opti-MEM™ as quantified from the gel electrophoresis using ImageJ software. (C) Size (number average) of the *Trans*IT-mRNA complexes dispersed in HEPES buffer by dynamic light scattering (DLS) at v/w ratio 2.

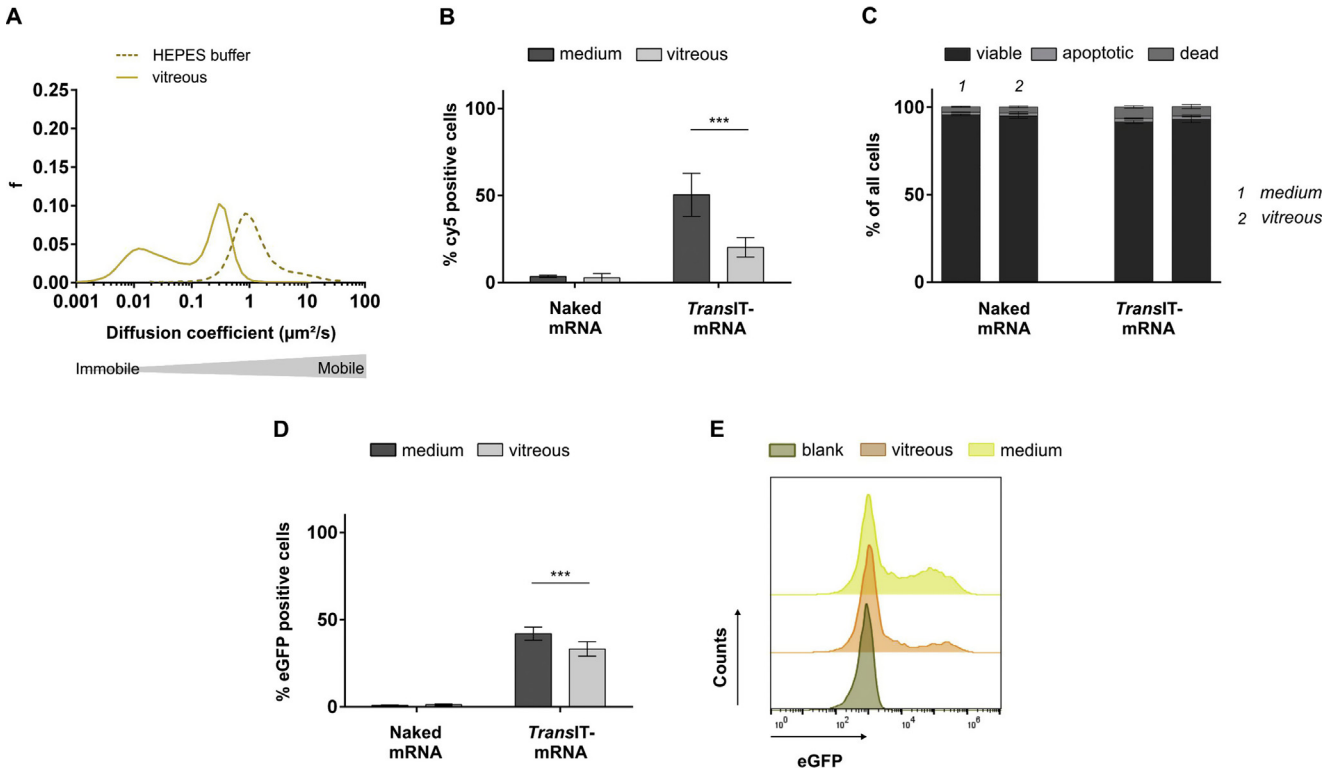


**Fig. 2. Influence of bovine vitreous on the mobility, uptake, toxicity and transfection efficiency of naked mRNA and *Trans*IT-complexed mRNA**. (A) Diffusion distributions of Cy5-labeled mRNA-*Trans*IT complexes in intact bovine vitreous humor (solid line), 24 h after IVT injection compared to their diffusion in HEPES buffer (dotted line). (B) Percentage of MIOM1 cells that display uptake after 3 h incubation with Cy5-labeled naked or complexed mRNA. (C) Cell viability 24 h after mRNA incubation with as quantified by flow cytometry. Untreated cells served as negative control. (D) Percentage of eGFP transfected MIOM1 Müller cells 24 h after incubation with naked and complexed mRNA. Representative flow cytometry histograms are shown in (E). Data is shown as mean ± SD ($n = 3$). ***, $p < 0.001$ medium versus vitreous by two-way ANOVA.

negative charges (Fig. 3A). When comparing the different MWs of HA, no substantial differences were seen in the size of the coated complexes. Interestingly, the higher the MW of the HA, the lower the zeta potential becomes when the same amount of HA monomers was added to the *Trans*IT-complexes (Fig. 3B). This indicates that addition of more HA monomers is necessary to provide stable negative complexes with HA22 or HA137 compared to HA2700. Since a HA/*Trans*IT/mRNA ratio of 16:2:1 (v/v/w) yields stable anionic particles and requires the least amount of HA monomers, this ratio was chosen for all following experiments.

To further confirm successful HA coating of the particles, the association of HA and mRNA to *Trans*IT was followed by fluorescence correlation spectroscopy (FCS). To this end the mRNA was labelled with YOYO-1 (green) and DyLight® 650-labelled HA22 (red) was used. The fluorescence of free HA, representing the negative control, was set at 100% (Fig. 3C, top row). Fig. 3C, middle row shows intense green fluorescence peaks in the fluctuation profiles of uncoated *Trans*IT-mRNA complexes, indicating dense packing of the fluorescent mRNA which corresponds to the presence of complexes. Following addition of red labelled HA to the complexes in a ratio of 16:2:1, the fluorescence baseline of HA dropped from 100% to 78%. As the baseline fluorescence correlates with the fraction of remaining free HA, this drop

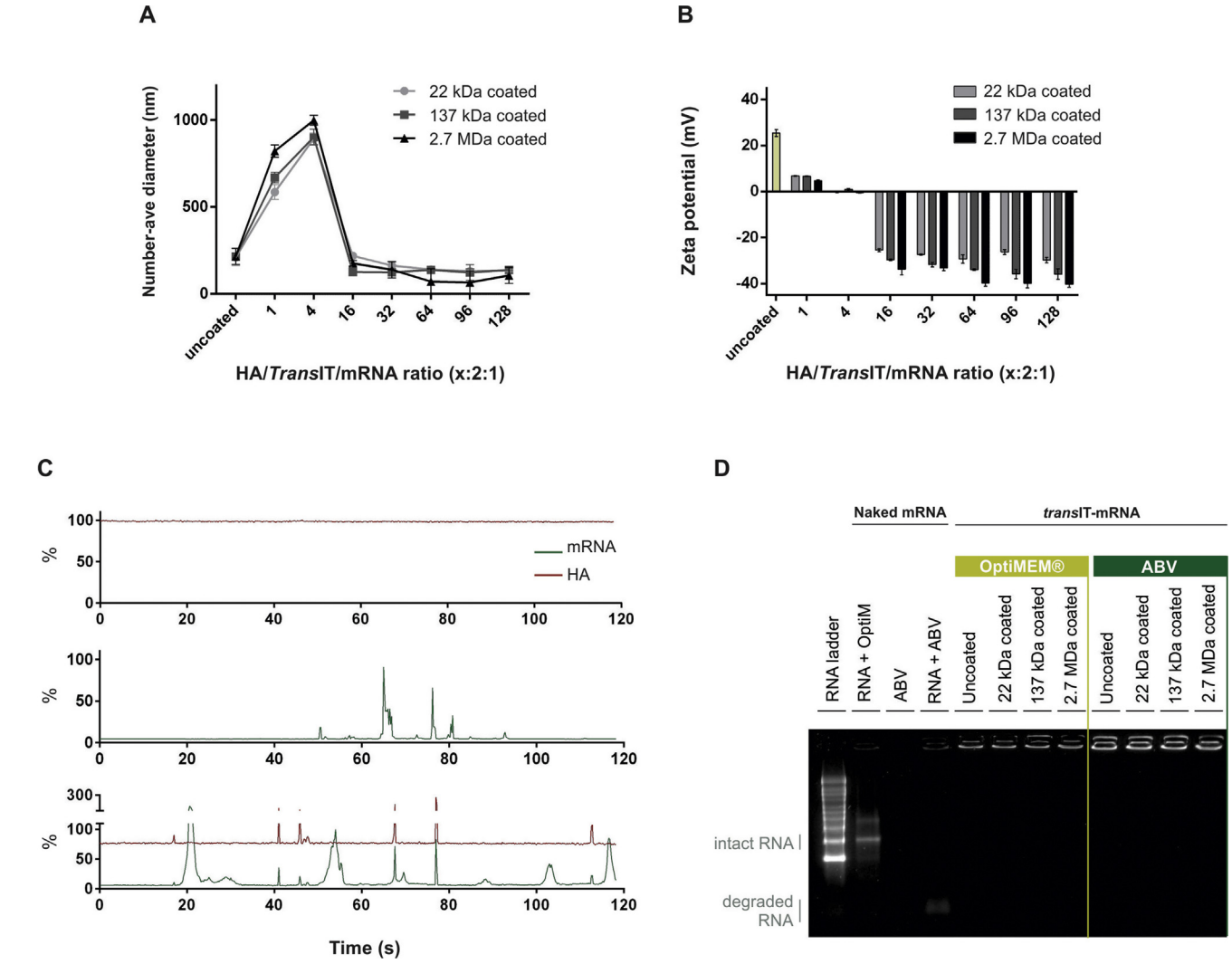


**Fig. 3. Physical characterization of HA-coated *Trans*IT-mRNA complexes.** Changes in size (number-averaged hydrodynamic diameter) (A) and zeta potential (B) after coating of *Trans*IT-mRNA complexes with HA in different ratios (ratio presents the number of negative charges originating from the carboxyl-group of the HA-monomer) and different molecular weights as measured by DLS in HEPES buffer. Data represent mean ± SD ($n$ = 3). (C) Representative fluorescence fluctuations of free HA (top row), uncoated *Trans*IT-complexed mRNA (middle row) and HA-coated *Trans*IT-complexed mRNA (16:2:1 v/v/w) (bottom row) as measured by fluorescence correlation spectroscopy (FCS) in HEPES buffer. (D) Gel electrophoresis on uncoated and HA-coated *Trans*IT-mRNA complexes demonstrates successful mRNA complexation after coating with different molecular weights of HA in both Opti-MEM™ and ABV. For (C) and (D) a charge ratio HA/*Trans*IT/mRNA of 16:2:1 (v/v/w) was used.

confirms binding of 22% of the HA to the complexes. In addition, peaks appeared in the red HA channel as well, co-occurring with the green mRNA fluorescence peaks (Fig. 3C, bottom row), demonstrating successful coating of the complexes with HA. It is important to note that some fluorescence peaks in the fluctuation profile of mRNA are not accompanied by a peak in the HA levels. These singular mRNA peaks may indicate that also a fraction of non-coated particles remains.

To assess whether the HA-coating influences the mRNA complexation capacity of the *Trans*IT, HA-coated complexes (ratio 16:2:1 (v/v/w)) were loaded on a 1% agarose gel. As can be seen from the results in Fig. 3D, HA-coating did not trigger mRNA release from the complexes at any MW. Hence, full encapsulation and protection of the mRNA is offered in both Opti-MEM™ and ABV at all MWs. Taken together, electrostatic coating of *Trans*IT-mRNA complexes results in stable, negatively charged particles, still able to fully protect the mRNA against degradation in bovine vitreous.

### 3.4. Improved vitreal mobility and transfection efficiency after coating with HA

After optimization we assessed whether HA-coating effectively improved the migration of *Trans*IT-mRNA complexes through the vitreous humor. Therefore, HA-coated (22 kDa, 137 kDa and 2700 kDa) complexes were injected in an *ex vivo* model containing intact vitreous and their mobility was compared to that of the uncoated complexes (Fig. 4A, black line) by fSPT microscopy. Diffusion coefficients of the different particles, established from their movement tracks, are displayed in Fig. 4A. Electrostatic coating of the *Trans*IT-mRNA complexes with HA clearly improved their mobility, with the highest increase in mobility seen for HA137. This outcome is likely attributed to the negative surface charge of the coated particles along with their smaller particle size (Fig. 4B). Indeed a substantial decrease in the amount of aggregated particles was seen following HA-coating, as demonstrated by the monodisperse (PDI < 0.3) size distribution.

The use of HA as an electrostatic surface coating of the *Trans*IT-mRNA complexes was further evaluated in its capacity to transfect MIOM1 Müller cells in the presence of sonicated bovine vitreous.

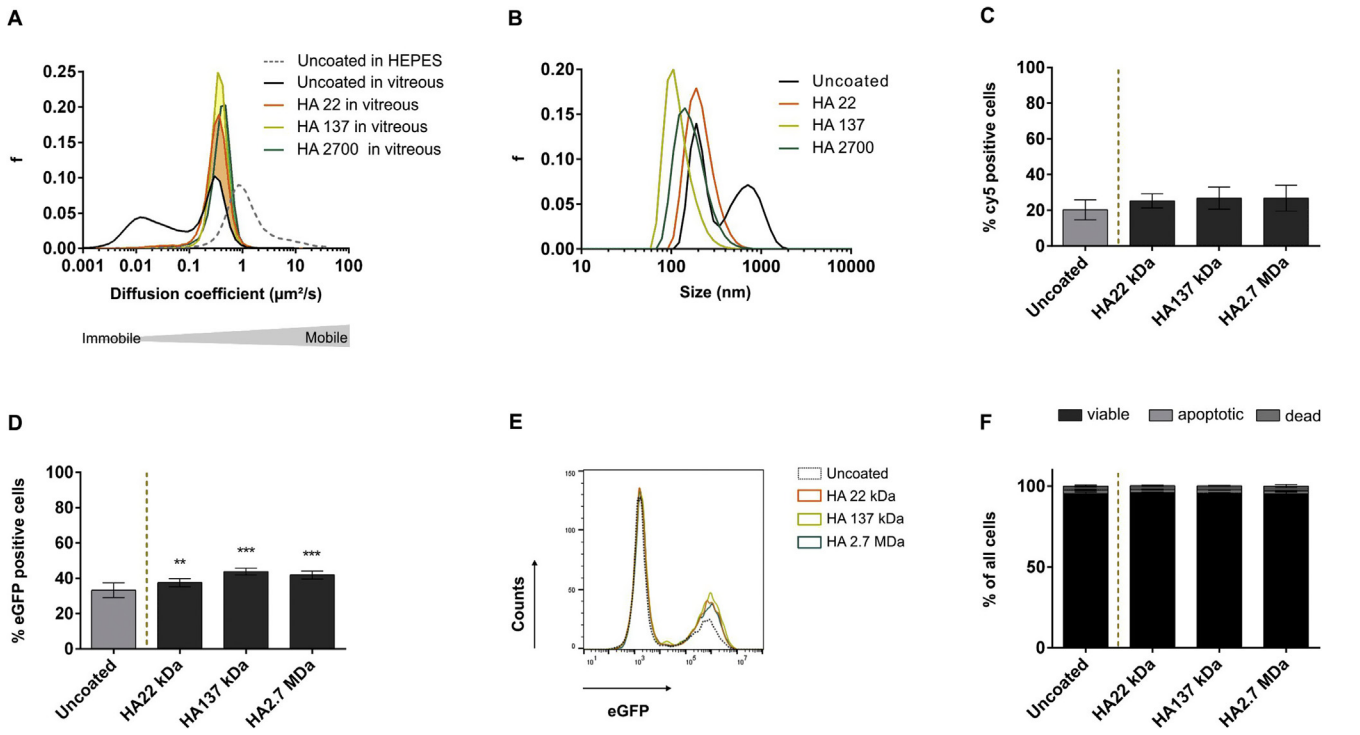


**Fig. 4. Influence of HA-coating on vitreal mobility, size, uptake, transfection efficiency and toxicity of *Trans*IT-complexed mRNA.** All measurements were done using a HA/*Trans*IT/mRNA ratio of 16. (A) Single particle tracking analysis of the IVT mobility of Cy5-labeled mRNA-*Trans*IT complexes before and after HA-coating with different molecular weights in intact bovine vitreous humor (solid lines), compared to the mobility of uncoated complexes in HEPES buffer (dotted line). Coating with 137 kDa HA resulted in the highest mobility increase. (B) Size (number average) of the coated *Trans*IT-mRNA complexes dispersed in HEPES buffer as measured by DLS. The size distribution of the uncoated complexes was added to the graph for comparison (solid black line). (C) Percentage of MIOM1 Müller cells that have taken up Cy5-labeled *Trans*IT-complexed mRNA 3 h after transfection. (D) Percentage of eGFP transfected MIOM1 Müller cells 24 h after incubation with *Trans*IT-complexed mRNA. Representative flow cytometry histograms are shown in (E). Cell viability after transfection evaluated by flow cytometry can be seen in F. Data is shown as mean ± SD ($n = 3$). $^{**}$, $p < 0.01$; $^{***}$, $p < 0.001$ coated versus uncoated by one-way ANOVA.

Fig. 4C shows that, despite a negative surface charge, HA-coated complexes are still taken up by the MIOM1 cells. Although no significant difference is seen in uptake, HA-coating with various MWs does slightly but significantly increase the transfection efficiency compared to the uncoated complexes (Fig. 4D,E). This modest increase was also noted when transfections were performed in culture medium rather than SV (Supplementary Fig. S2). Additionally, we examined the cytotoxicity of the coated and uncoated complexes in MIOM1 Müller cells by flow cytometry. As shown in Fig. 4F, no important cytotoxicity was observed for any of the complexes at the concentrations used for uptake and transfection analysis.

### 3.5. The ILM as a barrier for intravitreal mRNA delivery

Taken together, the preceding results show that HA137-coated *Trans*IT-mRNA complexes provide the highest mobility in bovine vitreous and are most proficient at inducing eGFP expression in MIOM1 cells *in vitro*. To determine their ability to cross the ILM and penetrate into the retina, we subsequently determined the localization of the mRNA complexed to HA137-coated *Trans*IT in a bovine retinal explant with vitreous attached [22]. This so-called 'vitreoretinal (VR) explant' keeps the VR interface intact and can be used to evaluate the transport of particles into the retina following IVT administration. HA137-coating of the complexes was performed as described before in a HA/*Trans*IT/mRNA ratio of 16:2:1 with Cy5-labeled eGFP mRNA. Twenty-four h after IVT injection, the HA137*Trans*IT-complexed mRNA (red) was able to migrate through the vitreous and a small fraction was present in the ganglion cell layer (GCL). However, the majority of the mRNA accumulated at the ILM (green) and could not penetrate into the neural retina (Fig. 5).

## 4. Discussion

IVT injection is a powerful administration route for a wide variety of drug delivery systems, since it is considered safe and circumvents several anterior barriers of the eye. Especially for the delivery of genetic information to the inner retina it is preferable to subretinal injection, since it provokes less retinal trauma and pathologic gliosis and could potentially generate a more wide-spread gene expression [6,11]. Yet, from the limited retinal transfection upon direct injection of these non-viral drug delivery systems into the vitreous humor, it is clear that specific barriers need to be overcome before achieving retinal transgene expression. Indeed, complexes need to efficiently diffuse through the vitreous and overcome the ILM before reaching the retina [41].

### 4.1. Overcoming the vitreal barrier

The first barrier encountered after IVT injection of mRNA is without any doubt the vitreous. The vitreous humor is composed of water (98–99%), salts, proteins (*e.g.* nucleases) and a complex network of randomly spaced collagen fibers and stabilizing glycosaminoglycans (GAGs), of which HA is the most abundant [28,45,46]. The presence of nucleases in the vitreous limits the applicability of naked mRNA injection due to enzymatic degradation of the mRNA, as seen in Fig. 1A. Therefore, we formulated the mRNA into particles by electrostatic complexation to a positively charged polymer/lipid formulation *Trans*IT, which was shown to protect mRNA against IVT hydrolysis (Fig. 1A). Unfortunately, mere protection of its cargo is not sufficient to ensure successful mRNA delivery to the retina. Our data show that at least a fraction of the *Trans*IT-mRNA complexes encounters difficulties while maneuvering through bovine vitreous (Fig. 2A). This observation

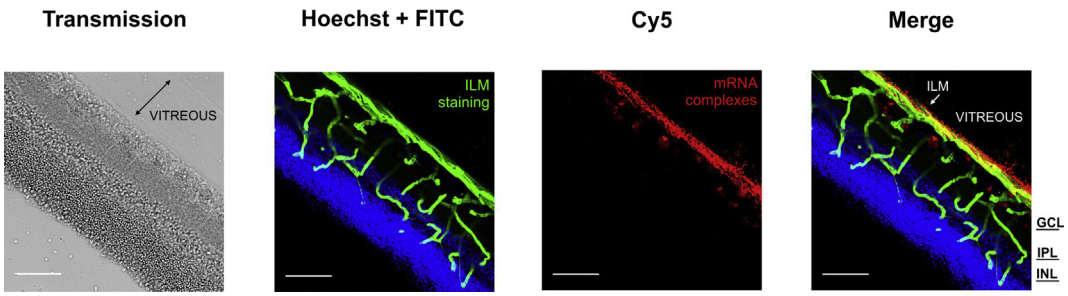


**Fig. 5. Confocal microscopy images of transverse retinal sections 24 h after IVT injection of Cy5-labeled *Trans*IT-complexed mRNA (red) injection in the vitreoretinal (VR) bovine explant.** The vitreous layer and ILM are indicated. ILM and retinal blood vessels are stained with anti-collagen antibodies (green), nuclei are stained with Hoechst (blue). (For interpretation of the references to colour in this figure legend, the reader is referred to the web version of this article.)

could be attributed to three factors. For one, there is a size limit for particle mobility through the vitreal network, which is estimated to be < 550 nm [15,25]. While the single particle fraction with sizes around 190 nm should be sufficiently small to move through the vitreous mesh, the aggregated fraction is likely too large (Fig. 1C). Secondly, the anionic nature of the vitreous, created by the presence of GAGs, can immobilize positively charged particles due to electrostatic adherence. This effect is even further enhanced by hydrophobic interactions which cause the particles to stick to the collagen fibrils [21,25]. Thirdly, reports have suggested the presence of an ocular "biomolecular corona". This is a layer of absorbed biomolecules, such as vitreal proteins that electrostatically interact with the particles [47]. This coating could increase the size of the complexes, thereby lowering their intravitreal mobility.

Furthermore, when *Trans*IT-complexed mRNA were added to MIOM1 Müller cells in the presence of sonicated vitreous, we observed a highly reduced uptake and transfection of MIOM1 cells in SV compared to culture medium (Fig. 2B,D-E), which is clearly not attributable to changes in cell viability (Fig. 2C). Therefore, we hypothesize that, although the vitreal network is mechanically broken up, the complexes interact with free GAGs, proteins and/or collagen remnants, which consequently limits intracellular uptake.

To prevent these electrostatic interactions with the vitreal constitutes, complexes can be coated with HA, an anionic, non-sulfated GAG, widely distributed throughout the vitreous humor of the eye [37,49]. *In vivo* HA usually occurs as a linear, high MW (up to $10^7$ kDa) polymer, yet enzymatic degradation can result in shorter fragments [30,50,51]. Extensive studies in mammals indicate that its physicochemical properties and functions are dependent on its MW, presumably due to the varying nature and affinity of its interactions with binding proteins and receptors (*e.g.* CD44) [36,51,52]. Upon addition of increasing amounts of HA to the cationic *Trans*IT-mRNA stable, negatively charged complexes were obtained from a HA/*Trans*IT/mRNA ratio of 16:2:1 (v/v/w) (Fig. 3A,B). Successful surface coating was subsequently confirmed by FCS analysis, where we demonstrate the presence of red-labeled HA on the surface of green-labeled mRNA complexes. As mRNA is complexed to the *Trans*IT reagent by spontaneous electrostatic interactions, addition of the anionic HA could cause a disruption of the complexes, leading to dissociation of the mRNA and subsequent degradation by vitreal RNases. Indeed, HA has been previously suggested to facilitate the release of DNA from nanoparticles consisting on solid lipid nanoparticles (SLNs) and protamine in HEK-293 cells [53]. However, gel electrophoresis experiments revealed that *Trans*IT-mRNA complexes remain stable in both Opti-MEM™ and bovine vitreous after coating with HA of all MWs (Fig. 3D).

Upon HA coating, the IVT mobility of the *Trans*IT-mRNA complexes substantially increased when compared to the mobility of the uncoated complexes, (Fig. 4A). This could be ascribed to two phenomena. Firstly, addition of HA prevents particle aggregation, which is supported by the more monodisperse size distributions of HA-coated versus uncoated particles in pure HEPES buffer (Fig. 4B). Indeed, all HA-coated formulations have an average size < 200 nm, which is lower than the estimated mesh size of the vitreal collagen network. Secondly, as the negative HA layer shields the cationic particles form electrostatic and hydrophobic interactions, attachment to the collagen fibrils as well as absorption of vitreal proteins (forming an 'unwanted' corona) could be prevented. Notably, the fraction of particles which was already mobile without any coating, was not altered in their diffusion. Therefore we hypothesize that this portion of uncoated particles is possibly mobilized due to spontaneous absorption of native HA on their cationic surface. Of all HA sizes, HA137 gave rise to the smallest HA-coated particles, and the highest frequency of mobile particles, in line with what has been reported by Martens et al. for the coating of polymer-based complexes [37]. Also Koo et al. investigated the movement of different nanoparticle types through the vitreous and demonstrated migration of self-assembled negatively charged HA nanoparticles through the collagen matrix and in the neural retina [19]. However, it is important to note that this last study was performed in rodents, of which the vitreous has a smaller volume and a more liquid composition [41,54,55]. Therefore, the impact of the vitreous barrier could be underestimated and care should be taken when extrapolating these data to larger animals and humans.

Interestingly, despite their negative surface charge, no difference in uptake was observed compared to uncoated complexes (Fig. 4B). This indicates that, although positively charged particles are generally expected to be endocytosed more efficiently due electrostatic binding to the cell membrane, other factors besides particle charge clearly influence cellular uptake. Uptake of HA-coated pDNA complexes, such as SLNs and cationic polyplexes, has been previously shown to be successful in ARPE-19 cells in presence of Opti-MEM™ [37,53]. In the same line, Hornof and de la Fuente demonstrated efficient uptake of HA-coated DNA/PEI polyplexes into human corneal epithelia cells, which was similar to the uncoated control [36]. As HA is an established ligand for the CD44-receptor, internalization of the coated complexes could be mediated by receptor-ligand interactions, as suggested by Martens et al. for RPE cells [37]. Indeed, the authors showed that saturation of the CD44 receptor by pre-incubation with free HA significantly reduced uptake of HA137-coated particles. Also Hornof et al. reported the uptake of their HA-coated complexes to be a receptor-mediated process, by antibody-mediated blockage of CD44 [36]. As the CD44 receptor is also present on the surface of Müller glia [56], receptor-mediated uptake could be a possible explanation for the observed results in this study. It can be argued however, whether this uptake mechanisms will still hold true following IVT injection *in vivo*, as, CD44 has been shown to be exclusively expressed on the apical side of Müller glia, facing towards the subretinal space [57]. *In vitro* situations, in which particles can come into contact with the entire Müller cell and not only the 'vitreal' side, should therefore be interpreted with necessary caution.

As previous studies by Mizrahi et al. and Wolny et al. reported a stronger binding of high MW HA (≥130 kDa) to the CD44 receptor [52,58], we expected a higher affinity and therefore increased uptake of the complexes with increasing HA size. However no significant

difference was observed in the uptake between the various MWs of HA in the present study. As the results of both previous reports were based on the immobilization of CD44 on a cell-free, planar support (at a 10–100 times higher density of CD44 receptors) caution should be taken, when comparing these results to our experiments performed on CD44-expressing cells. Nevertheless, also studies based on cell cultures showed a correlation between nanoparticle internalization and the size of the grafted HA chains, where uptake increased with increasing HA MW [59,60]. Differences in our results might be attributed to differences in CD44-receptor properties, as different cell types can have a different CD44-receptor density, clustering and turn-over rate, which can all lead to variations in HA-receptor interactions [30,37].

In contrast to carrier uptake, electrostatic HA-coating did slightly improve the transfection efficiency of the complexes in MIOM1 Müller cells, with HA137-coating producing the highest eGFP expression levels (Fig. 4C,D). This observation might be due to variations in intracellular trafficking and subsequent endosomal escape, as some studies claim that CD44 receptor-mediated uptake is able to avoid lysosomal degradation leading to higher transfection efficiencies [61,62]. Also, it might be possible that HA coating favors the dissociation of mRNA from the complexes, leading to more efficient intracellular release of mRNA into the cytoplasm.

### 4.2. Retinal delivery impairment due to ILM

Apart from the vitreous, an equally important barrier for mRNA delivery to the retina is the ILM. The ILM serves as the structural interface between the vitreous body and the retina and mainly consists of collagen type IV, laminin and heparin sulfate proteoglycans which form a complex sheet-like network by specific crosslink interactions [44]. Several reports have demonstrated that the ILM is a critical barrier impeding both viral and non-viral vectors to reach the retina after IVT injection [19,63–67]. To evaluate whether *Trans*IT-complexed mRNA is able to overcome the ILM after IVT injection, we made use of a VR explant model, which guarantees an intact ILM by keeping the vitreous attached to the retina at all times [22]. To this end, we made use of HA137-coated *Trans*IT particles as (1) negatively charged particles have previously been reported to cross the ILM, while cationic ones are drastically hindered in their penetration [19]; (2) HA137-coating yielded the best improvement in vitreal mobility and (3) produced the highest levels of eGFP expression in MIOM1 Müller cells. The majority of the HA coated particles clearly accumulated at the ILM (Fig. 5), although based on previous reports, we expected that at least part of the negatively charged HA-complexes would penetrate into the retina [19,66,67]. Indeed, it is generally accepted in both rodent as well as bovine eyes, that predominantly positively charged particles are hindered by the ILM, while neutral to negatively charged are able to pass [41]. In addition, also their particle size of ~110 nm (Fig. 4B) suggested successful transport through the ILM, as various studies demonstrated efficient entry of larger particles into the retina. For instance, the research group of Rodríguez-Gascón found SLNs up to 230 nm in size to induce eGFP expression throughout the entire mice retina after IVT injection [68]. Likewise, Bourges et al. reported transretinal movement of 310 nm sized neutral polylactide particles following injection into the rat vitreous [18]. Notably, even negatively charged particles of 350 nm were shown to efficiently penetrate the healthy retina of rats [19]. An important difference with our experiments, however, is that the aforementioned studies were performed in rodents which are known to have a simplified ILM structure, that is underdeveloped and only shows similarities with the fetal human ILM [44]. In contrast, a recent study of Peynshaert et al., applying the same model as used in this study, demonstrated that 100 and 200 nm sized anionic polystyrene beads had difficulties overcoming the bovine ILM [22]. This is in line with our results, as we see a only very limited retinal entry of the mRNA, which is moreover restricted to the RGL (Fig. 5). These findings highlight the importance of experimenting on ocular tissue of larger, more relevant species (*e.g.,* cow, pig, non-human primates or even human eyes) to provide results that are more predictable for the human situation.

It should be noted that several methods to improve transport across the ILM have been proposed in literature. Dalkara et al., for example, demonstrated that enzymatic lysis of the ILM induced by protease treatment substantially increased retinal transduction of various intravitreally injected AAV serotypes [69]. Similarly, recent studies in non-human primates demonstrated the power of surgical ILM peeling on retina penetration of AAV2 vectors, which clearly resulted in a larger area and higher intensity of retinal GFP expression [70,71]. Finally, also laser photocoagulation pretreatment was shown to improve viral transduction of the mice retina, presumably caused by cell stress response and upregulation of capsid receptors [72]. Whether or not the use of these ILM manipulation techniques will be necessary in the diseased retina, in which the ILM might be breached during retinal degeneration, remains to be seen [60,73,74].

## 5. Conclusion

Although there are multiple benefits in the use of mRNA for the expression of therapeutic proteins in the retina, this study clearly shows the critical challenge of delivering mRNA-based therapeutics to their target site. Especially when IVT injection is desired in order to reach the inner retina, the vitreous and ILM represent major gene delivery barriers. In this study we demonstrated that smart adjustments of a predefined mRNA carrier such as electrostatic coating with HA can provide the desired physicochemical characteristics to overcome the vitreal barrier. Unfortunately, these modifications were not sufficient to ensure retinal penetration, as the particles accumulated at the ILM. In contrast to various studies demonstrating ILM penetration of similar or bigger sized negatively charged particles in rodents, we found the ILM to be the predominant barrier impeding particle transfer to the bovine retina. This work therefore encourages systematic studies into particle properties for successful retinal entry in larger species such as cows, pigs or even humans.

## Acknowledgements

Joke Devoldere is a doctoral fellow of the Research Foundation-Flanders, Belgium (FWO-Vlaanderen). Karen Peynshaert and Heleen Dewitte are post-doctoral fellow of FWO-Vlaanderen. This work was further funded by an award granted by Funding for Research in Ophthalmology (FRO). The authors would like to thank George Dakwar and Toon Brans for their help with the fSPT and confocal microscopy experiments. Finally the kind people of Flanders Meat Group in Zele are acknowledged for the freshly enucleated cow eyes.

## Appendix A. Supplementary material

Supplementary data to this article can be found online at https://doi.org/10.1016/j.ejpb.2019.05.023.

## References

[1] J. Devoldere, H. Dewitte, S.C. De Smedt, K. Remaut, Evading innate immunity in nonviral mRNA delivery: don't shoot the messenger, Drug Discovery Today 21 (2016) 11–25.
[2] C. Leonhardt, G. Schwake, T.R. Stogbauer, S. Rappl, J.T. Kuhr, T.S. Ligon, J.O. Radler, Single-cell mRNA transfection studies: delivery, kinetics and statistics by numbers, Nanomed. : Nanotechnol. Biol. Med. 10 (2014) 679–688.
[3] U. Sahin, K. Kariko, O. Tureci, mRNA-based therapeutics–developing a new class of drugs, Nat. Rev. Drug Discov. 13 (2014) 759–780.
[4] W.A. Hare, E. WoldeMussie, R.K. Lai, H. Ton, G. Ruiz, T. Chun, L. Wheeler, Efficacy and safety of memantine treatment for reduction of changes associated with experimental glaucoma in monkey, I: Functional measures, Invest. Ophthalmol. Vis. Sci. 45 (2004) 2625–2639.
[5] H. Shan, D. Ji, A.R. Barnard, D.M. Lipinski, Q. You, E.J. Lee, T.A. Kamalden, X. Sun, R.E. MacLaren, AAV-mediated gene transfer of human X-linked inhibitor of

apoptosis protects against oxidative cell death in human RPE cells, Invest. Ophthalmol. Vis. Sci. 52 (2011) 9591–9597.
[6] D. Dalkara, K.D. Kolstad, K.I. Guerin, N.V. Hoffmann, M. Visel, R.R. Klimczak, D.V. Schaffer, J.G. Flannery, AAV mediated GDNF secretion from retinal glia slows down retinal degeneration in a rat model of retinitis pigmentosa, Mol. Therapy : J. Am. Soc. Gene Therapy 19 (2011) 1602–1608.
[7] L.C. Byrne, D. Dalkara, G. Luna, S.K. Fisher, E. Clerin, J.A. Sahel, T. Leveillard, J.G. Flannery, Viral-mediated RdCVF and RdCVFL expression protects cone and rod photoreceptors in retinal degeneration, J. Clin. Invest. 125 (2015) 105–116.
[8] R.E. MacLaren, P.K. Buch, A.J. Smith, K.S. Balaggan, A. MacNeil, J.S. Taylor, N.N. Osborne, R.R. Ali, CNTF gene transfer protects ganglion cells in rat retinae undergoing focal injury and branch vessel occlusion, Exp. Eye Res. 83 (2006) 1118–1127.
[9] V. Haurigot, P. Villacampa, A. Ribera, A. Bosch, D. Ramos, J. Ruberte, F. Bosch, Long-term retinal PEDF overexpression prevents neovascularization in a murine adult model of retinopathy, PloS One 7 (2012) e41511.
[10] D.M. Lipinski, A.R. Barnard, M.S. Singh, C. Martin, E.J. Lee, W.I.L. Davies, R.E. MacLaren, CNTF gene therapy confers lifelong neuroprotection in a mouse model of human retinitis pigmentosa, Mol. Therapy : J. Am. Soc. Gene Therapy 23 (2015) 1308–1319.
[11] R. Da Costa, C. Roger, J. Segelken, M. Barben, C. Grimm, J. Neidhardt, A Novel method combining vitreous aspiration and intravitreal AAV2/8 injection results in retina-wide transduction in adult mice, Invest. Ophthalmol. Vis. Sci. 57 (2016) 5326–5334.
[12] E. Fattal, A. Bochot, Ocular delivery of nucleic acids: antisense oligonucleotides, aptamers and siRNA, Adv. Drug Deliv. Rev. 58 (2006) 1203–1223.
[13] J. Adijanto, M.I. Naash, Nanoparticle-based technologies for retinal gene therapy, Eur. J. Pharmaceut. Biopharmaceut.: Off. J. Arbeitsgemeinschaft fur Pharmazeutische Verfahrenstechnik e.V 95 (2015) 353–367.
[14] R. Zulliger, S.M. Conley, M.I. Naash, Non-viral therapeutic approaches to ocular diseases: An overview and future directions, J. Control. Release : Off. J. Control. Release Soc. 219 (2015) 471–487.
[15] L. Peeters, N.N. Sanders, K. Braeckmans, K. Boussery, J. Van de Voorde, S.C. De Smedt, J. Demeester, Vitreous: a barrier to nonviral ocular gene therapy, Invest. Ophthalmol. Vis. Sci. 46 (2005) 3553–3561.
[16] J. Mains, C.G. Wilson, The vitreous humor as a barrier to nanoparticle distribution, J. Ocul. Pharmacol. Th. 29 (2013) 143–150.
[17] C.L. Rowe-Rendleman, S.A. Durazo, U.B. Kompella, K.D. Rittenhouse, A. Di Polo, A.L. Weiner, H.E. Grossniklaus, M.I. Naash, A.S. Lewin, A. Horsager, H.F. Edelhauser, Drug and gene delivery to the back of the eye: from bench to bedside, Invest. Ophthalmol. Vis. Sci. 55 (2014) 2714–2730.
[18] J.L. Bourges, S.E. Gautier, F. Delie, R.A. Bejjani, J.C. Jeanny, R. Gurny, D. BenEzra, F.F. Behar-Cohen, Ocular drug delivery targeting the retina and retinal pigment epithelium using polylactide nanoparticles, Invest. Ophthalmol. Vis. Sci. 44 (2003) 3562–3569.
[19] H. Koo, H. Moon, H. Han, J.H. Na, M.S. Huh, J.H. Park, S.J. Woo, K.H. Park, I.C. Kwon, K. Kim, H. Kim, The movement of self-assembled amphiphilic polymeric nanoparticles in the vitreous and retina after intravitreal injection, Biomaterials 33 (2012) 3485–3493.
[20] I. Trapani, S. Banfi, F. Simonelli, E.M. Surace, A. Auricchio, Gene therapy of inherited retinal degenerations: prospects and challenges, Hum. Gene Ther. 26 (2015) 193–200.
[21] T.F. Martens, D. Vercauteren, K. Forier, H. Deschout, K. Remaut, R. Paesen, M. Ameloot, J.F. Engbersen, J. Demeester, S.C. De Smedt, K. Braeckmans, Measuring the intravitreal mobility of nanomedicines with single-particle tracking microscopy, Nanomedicine (Lond) 8 (2013) 1955–1968.
[22] K. Peynshaert, J. Devoldere, V. Forster, S. Picaud, C. Vanhove, S.C. De Smedt, K. Remaut, Toward smart design of retinal drug carriers: a novel bovine retinal explant model to study the barrier role of the vitreoretinal interface, Drug Deliv. 24 (2017) 1384–1394.
[24] L. Pitkanen, M. Ruponen, J. Nieminen, A. Urtti, Vitreous is a barrier in nonviral gene transfer by cationic lipids and polymers, Pharm. Res. 20 (2003) 576–583.
[25] Q. Xu, N.J. Boylan, J.S. Suk, Y.Y. Wang, E.A. Nance, J.C. Yang, P.J. McDonnell, R.A. Cone, E.J. Duh, J. Hanes, Nanoparticle diffusion in, and microrheology of, the bovine vitreous ex vivo, J. Control. Release : Off. J. Control. Release Soc. 167 (2013) 76–84.
[26] N.N. Sanders, L. Peeters, I. Lentacker, J. Demeester, S.C. De Smedt, Wanted and unwanted properties of surface PEGylated nucleic acid nanoparticles in ocular gene transfer, J. Control. Release : Off. J. Control. Release Soc. 122 (2007) 226–235.
[27] S. Mishra, P. Webster, M.E. Davis, PEGylation significantly affects cellular uptake and intracellular trafficking of non-viral gene delivery particles, Eur. J. Cell Biol. 83 (2004) 97–111.
[28] P.N. Bishop, Structural macromolecules and supramolecular organisation of the vitreous gel, Progress Retinal Eye Res. 19 (2000) 323–344.
[29] S.J. Clark, T.D. Keenan, H.L. Fielder, L.J. Collinson, R.J. Holley, C.L. Merry, T.H. van Kuppevelt, A.J. Day, P.N. Bishop, Mapping the differential distribution of glycosaminoglycans in the adult human retina, choroid, and sclera, Invest. Ophthalmol. Vis. Sci. 52 (2011) 6511–6521.
[30] M. Guter, M. Breunig, Hyaluronan as a promising excipient for ocular drug delivery, Eur. J. Pharm. Biopharm. 113 (2017) 34–49.
[36] M. Hornof, M. de la Fuente, M. Hallikainen, R.H. Tammi, A. Urtti, Low molecular weight hyaluronan shielding of DNA/PEI polyplexes facilitates CD44 receptor mediated uptake in human corneal epithelial cells, J. Gene Med. 10 (2008) 70–80.
[37] T.F. Martens, K. Remaut, H. Deschout, J.F.J. Engbersen, W.E. Hennink, M.J. van Steenbergen, J. Demeester, S.C. De Smedt, K. Braeckmans, Coating nanocarriers with hyaluronic acid facilitates intravitreal drug delivery for retinal gene therapy, J. Control. Release 202 (2015) 83–92.
[38] J. Devoldere, K. Peynshaert, S.C. De Smedt, K. Remaut, Muller cells as a target for retinal therapy, Drug Discov. Today (2019).
[39] K. Braeckmans, K. Buyens, W. Bouquet, C. Vervaet, P. Joye, F. De Vos, L. Plawinski, L. Doeuvre, E. Angles-Cano, N.N. Sanders, J. Demeester, S.C. De Smedt, Sizing nanomatter in biological fluids by fluorescence single particle tracking, Nano Lett. 10 (2010) 4435–4442.
[40] G.A. Limb, T.E. Salt, P.M. Munro, S.E. Moss, P.T. Khaw, In vitro characterization of a spontaneously immortalized human Muller cell line(MIO-M1), Invest. Ophthalmol. Vis. Sci. 43 (2002) 864–869.
[41] K. Peynshaert, J. Devoldere, S.C. De Smedt, K. Remaut, In vitro and ex vivo models to study drug delivery barriers in the posterior segment of the eye, Adv. Drug Deliv. Rev. (2017).
[44] K. Peynshaert, J. Devoldere, A.K. Minnaert, S.C. De Smedt, K. Remaut, Morphology and composition of the inner limiting membrane: species-specific variations and relevance toward drug delivery research, Curr. Eye Res. (2019) 1–11.
[45] M.M. Le Goff, P.N. Bishop, Adult vitreous structure and postnatal changes, Eye 22 (2008) 1214–1222.
[46] M.T. Ahmad, P. Zhang, C. Dufresne, L. Ferrucci, R.D. Semba, The human eye proteome project: updates on an emerging proteome, Proteomics 18 (2018) e1700394.
[47] D.H. Jo, J.H. Kim, J.G. Son, K.S. Dan, S.H. Song, T.G. Lee, J.H. Kim, Nanoparticle-protein complexes mimicking corona formation in ocular environment, Biomaterials 109 (2016) 23–31.
[49] J.R. Fraser, T.C. Laurent, U.B. Laurent, Hyaluronan: its nature, distribution, functions and turnover, J. Intern. Med. 242 (1997) 27–33.
[50] Y.H. Liao, S.A. Jones, B. Forbes, G.P. Martin, M.B. Brown, Hyaluronan: Pharmaceutical characterization and drug delivery, Drug Deliv. 12 (2005) 327–342.
[51] R. Stern, A.A. Asari, K.N. Sugahara, Hyaluronan fragments: an information-rich system, Eur. J. Cell Biol. 85 (2006) 699–715.
[52] S. Mizrahy, S.R. Raz, M. Hasgaard, H. Liu, N. Soffer-Tsur, K. Cohen, R. Dvash, D. Landsman-Milo, M.G. Bremer, S.M. Moghimi, D. Peer, Hyaluronan-coated nanoparticles: the influence of the molecular weight on CD44-hyaluronan interactions and on the immune response, J. Control. Release : Off. J. Control. Release Soc. 156 (2011) 231–238.
[53] P.S. Apaolaza, D. Delgado, A. del Pozo-Rodriguez, A.R. Gascon, M.A. Solinis, A novel gene therapy vector based on hyaluronic acid and solid lipid nanoparticles for ocular diseases, Int. J. Pharm. 465 (2014) 413–426.
[54] J.M. Skeie, S.H. Tsang, V.B. Mahajan, Evisceration of mouse vitreous and retina for proteomic analyses, Jove-J. Vis. Exp. (2011).
[55] E.M. Del Amo, A.K. Rimpela, E. Heikkinen, O.K. Kari, E. Ramsay, T. Lajunen, M. Schmitt, L. Pelkonen, M. Bhattacharya, D. Richardson, A. Subrizi, T. Turunen, M. Reinisalo, J. Itkonen, E. Toropainen, M. Casteleijn, H. Kidron, M. Antopolsky, K.S. Vellonen, M. Ruponen, A. Urtti, Pharmacokinetic aspects of retinal drug delivery, Progress Retinal Eye Res. 57 (2017) 134–185.
[56] T. Shinoe, H. Kuribayashi, H. Saya, M. Seiki, H. Aburatani, S. Watanabe, Identification of CD44 as a cell surface marker for Muller glia precursor cells, J. Neurochem 115 (2010) 1633–1642.
[57] L.K. Too, G. Gracie, E. Hasic, J.H. Iwakura, S. Cherepanoff, Adult human retinal Muller glia display distinct peripheral and macular expression of CD117 and CD44 stem cell-associated proteins, Acta Histochem. 119 (2017) 142–149.
[58] P.M. Wolny, S. Banerji, C. Gounou, A.R. Brisson, A.J. Day, D.G. Jackson, R.P. Richter, Analysis of CD44-hyaluronan interactions in an artificial membrane system: insights into the distinct binding properties of high and low molecular weight hyaluronan, J. Biol. Chem. 285 (2010) 30170–30180.
[59] H.S.S. Qhattal, X.L. Liu, Characterization of CD44-mediated cancer cell uptake and intracellular distribution of hyaluronan-grafted liposomes, Mol. Pharmaceut. 8 (2011) 1233–1246.
[60] L. Gan, J. Wang, Y.N. Zhao, D. Chen, C.L. Zhu, J.P. Liu, Y. Gan, Hyaluronan-modified core-shell liponanoparticles targeting CD44-positive retinal pigment epithelium cells via intravitreal injection, Biomaterials 34 (2013) 5978–5987.
[61] L. Contreras-Ruiz, M. de la Fuente, J.E. Parraga, A. Lopez-Garcia, I. Fernandez, B. Seijo, A. Sanchez, M. Calonge, Y. Diebold, Intracellular trafficking of hyaluronic acid-chitosan oligomer-based nanoparticles in cultured human ocular surface cells, Mol. Vision 17 (2011) 279–290.
[62] S.L. Hayward, C.L. Wilson, S. Kidambi, Hyaluronic acid-conjugated liposome nanoparticles for targeted delivery to CD44 overexpressing glioblastoma cells, Oncotarget 7 (2016) 34158–34171.
[63] M. Hellstrom, M.J. Ruitenberg, M.A. Pollett, E.M. Ehlert, J. Twisk, J. Verhaagen, A.R. Harvey, Cellular tropism and transduction properties of seven adeno-associated viral vector serotypes in adult retina after intravitreal injection, Gene Ther. 16 (2009) 521–532.
[64] R.E. Boyd, D.G. Sledge, S.L. Boye, S.E. Boye, W.W. Hauswirth, A.M. Komaromy, S.M. Petersen-Jones, J.T. Bartoe, Photoreceptor-targeted gene delivery using intravitreally administered AAV vectors in dogs, Gene Ther. 23 (2016) 223–230.
[65] F.M. Mowat, K.R. Gornik, A. Dinculescu, S.L. Boye, W.W. Hauswirth, S.M. Petersen-Jones, J.T. Bartoe, Tyrosine capsid-mutant AAV vectors for gene delivery to the canine retina from a subretinal or intravitreal approach, Gene Ther. 21 (2014) 96–105.
[66] L. Pitkanen, J. Pelkonen, M. Ruponen, S. Ronkko, A. Urtti, Neural retina limits the nonviral gene transfer to retinal pigment epithelium in an in vitro bovine eye model, AAPS J. 6 (2004) e25.
[67] J. Lee, U. Goh, H.J. Lee, J. Kim, M. Jeong, J.H. Park, Effective retinal penetration of lipophilic and lipid-conjugated hydrophilic agents delivered by engineered liposomes, Mol. Pharm. 14 (2017) 423–430.
[68] P.S. Apaolaza, A. Del Pozo-Rodriguez, M.A. Solinis, J.M. Rodriguez, U. Friedrich, J. Torrecilla, B.H. Weber, A. Rodriguez-Gascon, Structural recovery of the retina in

a retinoschisin-deficient mouse after gene replacement therapy by solid lipid nanoparticles, Biomaterials 90 (2016) 40–49.
[69] D. Dalkara, K.D. Kolstad, N. Caporale, M. Visel, R.R. Klimczak, D.V. Schaffer, J.G. Flannery, Inner limiting membrane barriers to AAV-mediated retinal transduction from the vitreous, Mol. Therapy : J. Am. Soc. Gene Therapy 17 (2009) 2096–2102.
[70] K. Takahashi, T. Igarashi, K. Miyake, M. Kobayashi, C. Yaguchi, O. Iijima, Y. Yamazaki, Y. Katakai, N. Miyake, S. Kameya, T. Shimada, H. Takahashi, T. Okada, Improved intravitreal AAV-mediated inner retinal gene transduction after surgical internal limiting membrane peeling in cynomolgus monkeys, Mol. Therapy : J. Am. Soc. Gene Therapy 25 (2017) 296–302.
[71] K.Y.C. Teo, S.Y. Lee, A.V. Barathi, S.B.B. Tun, L. Tan, I.J. Constable, Surgical removal of internal limiting membrane and layering of AAV vector on the retina under air enhances gene transfection in a nonhuman primate, Invest. Ophthalmol. Vis. Sci. 59 (2018) 3574–3583.
[72] S.H. Lee, P. Colosi, H. Lee, Y.H. Ohn, S.W. Kim, H.W. Kwak, T.K. Park, Laser photocoagulation enhances adeno-associated viral vector transduction of mouse retina, Hum. Gene Ther. Method 25 (2014) 83–91.
[73] K.D. Kolstad, D. Dalkara, K. Guerin, M. Visel, N. Hoffmann, D.V. Schaffer, J.G. Flannery, Changes in adeno-associated virus-mediated gene delivery in retinal degeneration, Hum. Gene Ther. 21 (2010) 571–578.
[74] O. Vacca, M. Darche, D.V. Schaffer, J.G. Flannery, J.A. Sahel, A. Rendon, D. Dalkara, AAV-mediated gene delivery in Dp71-null mouse model with compromised barriers, Glia 62 (2014) 468–476.